





Article

# Fate of Hydrocarbons in Iron-Bearing Mineral Environments during Subduction

Aleksandr Serovaiskii <sup>1,\*</sup>, Elena Mukhina <sup>2</sup>, Leonid Dubrovinsky <sup>3</sup>, Aleksey Chernoutsan <sup>1</sup>, Daniil Kudryavtsev <sup>4</sup>, Catherine McCammon <sup>3</sup>, Georgios Aprilis <sup>5</sup>, Ilya Kupenko <sup>6</sup>, Aleksandr Chumakov <sup>7</sup>, Michael Hanfland <sup>7</sup> and Vladimir Kutcherov <sup>1,4,8</sup>

<sup>1</sup> Department of Physics, Gubkin Russian State University of Oil and Gas (National Research University), Leninskiy avenue 65/1, 119991 Moscow, Russia

<sup>2</sup> Skolkovo Institute of Science and Technology, Bolshoy Boulevard 30, bld. 1, 121205 Moscow, Russia

<sup>3</sup> Bayerisches Geoinstitut, Universität Bayreuth, Universitätsstraße 30, 95440 Bayreuth, Germany

<sup>4</sup> Department of Energy Technology, KTH Royal Institute of Technology, Brinellvägen 68, 10044 Stockholm, Sweden

<sup>5</sup> Materials Physics and Technology at Extreme Conditions, Laboratory of Crystallography, Universität Bayreuth, D-95440 Bayreuth, Germany

<sup>6</sup> The Institute for Mineralogy of the Westfälische Wilhelms, Universität Münster, Corrensstraße 24, 48149 Münster, Germany

<sup>7</sup> ESRF-The European Synchrotron, CS40220 38043 Grenoble Cedex 9, France

<sup>8</sup> Department of Industrial Economy and Management, KTH Royal Institute of Technology, Lindstedtsvägen 30, 11428 Stockholm, Sweden

\* Correspondence: alexandrserov@gmail.com; Tel.: +7-9096394699

Received: 10 September 2019; Accepted: 18 October 2019; Published: 23 October 2019



**Abstract:** Subducted sediments play a key role in the evolution of the continental crust and upper mantle. As part of the deep carbon cycle, hydrocarbons are accumulated in sediments of subduction zones and could eventually be transported with the slab below the crust, thus affecting processes in the deep Earth's interior. However, the behavior of hydrocarbons during subduction is poorly understood. We experimentally investigated the chemical interaction of model hydrocarbon mixtures or natural oil with ferrous iron-bearing silicates and oxides (representing possible rock-forming materials) at pressure-temperature conditions of the Earth's lower crust and upper mantle (up to 2000(±100) K and 10(±0.2) GPa), and characterized the run products using Raman and Mössbauer spectroscopies and X-ray diffraction. Our results demonstrate that complex hydrocarbons are stable on their own at thermobaric conditions corresponding to depths exceeding 50 km. We also found that chemical reactions between hydrocarbons and ferrous iron-bearing rocks during slab subduction lead to the formation of iron hydride and iron carbide. Iron hydride with relatively low melting temperature may form a liquid with negative buoyancy that could transport reduced iron and hydrogen to greater depths.

**Keywords:** iron carbide; iron hydride; subduction; hydrocarbons; petroleum; mantle

## 1. Introduction

Subduction processes are involved in the deep carbon cycle through the transport of carbon between the Earth's surface and its interior. In subducting slabs, carbon is usually considered to be in the form of organic carbon in sediments [1], carbonates [2,3], and pure crystalline graphite [3]. Known carbon species in the Earth's interior are CO<sub>2</sub> and CH<sub>4</sub> fluid or gas [4,5], diamond [1,6], carbonates [2,3], carbides [7], and carbonated silicate melts [4]. Petroleum as a carbon-containing substance within subducting slabs has not been strongly considered. However, numerous giant petroleum deposits are

located close to subduction zones [8] and there are no compelling reasons to exclude the involvement of hydrocarbons in subduction.

During subduction, petroleum hydrocarbons may be released from the reservoir rock individually and in connection with reservoir minerals and could chemically interact (faster or slower depending on their aggregate state and pressure-temperature conditions) with surrounding minerals at the corresponding thermodynamic conditions. Consequently, it is expected that petroleum-containing rocks will experience increasing pressures and temperatures, starting from ambient (at the surface) to 2000( $\pm$ 100) K and 10( $\pm$ 0.2) GPa (at 300 km depth), representing the slab and surrounding mantle conditions [9].

What do we know about the stability of complex hydrocarbon systems at thermobaric conditions of the Earth's crust and the upper mantle? First, a number of supergiant petroleum deposits have been discovered down to depths of 11 km [10]. Second, experimental data (see Figure S1) indicate that complex hydrocarbons are stable up to thermobaric conditions corresponding to depths of 50 km (723( $\pm$ 10) K and 1.4( $\pm$ 0.2) GPa) [11]. Third, it was demonstrated that a natural gas-like system could be reversibly formed from individual saturated hydrocarbons [12], or from different donors of carbon and hydrogen [13,14] in the temperature range of 1000 K to 1500 K and at pressures above 2 GPa (which corresponds to the pT parameters of slabs at 80–150 km depths) with simultaneous oxidation of Fe or FeO to Fe<sub>3</sub>O<sub>4</sub>. These observations suggest that (a) pressure and temperature alone cannot destabilize petroleum at the lower crust and upper mantle conditions, and (b) iron may play an important role in the fate of hydrocarbons in the Earth's interior.

Iron is the most important element in subduction zones with a variable valence state and is expected to control the oxygen fugacity of corresponding processes [15]. Thus, we have investigated whether interaction with iron-bearing minerals in subducting slabs or in mantle rocks may affect the behavior of hydrocarbons.

## 2. Materials and Methods

### 2.1. Samples

As a source of hydrocarbons, we used paraffin oil (99,9% purity, see Table S1) and crude oil (Korchaginское deposit, Astrakhan region) (see Table S2) (while crude oil shows strong luminescence which interferes with Raman spectroscopy, paraffin oil does not have this limitation).

As iron-bearing materials we used pyroxene-like glass with composition (Mg<sub>0.91</sub>Fe<sub>0.09</sub>)(Si<sub>0.91</sub>Al<sub>0.09</sub>)O<sub>3</sub>, ferropericlase (Mg<sub>0.8</sub>Fe<sub>0.2</sub>)O, and wüstite Fe<sub>0.94</sub>O. The synthesis of powdered <sup>57</sup>Fe-enriched ferropericlase (Mg<sub>0.8</sub><sup>57</sup>Fe<sub>0.2</sub>)O is described in [16]. Powder of <sup>57</sup>Fe-enriched pyroxene-like glass (Mg<sub>0.91</sub>Fe<sub>0.09</sub>Si<sub>0.91</sub>Al<sub>0.09</sub>)O<sub>3</sub> was synthesized using a 1-atmosphere box furnace from a pelletized mixture of Fe<sub>2</sub>O<sub>3</sub>, Mg(OH)<sub>2</sub>, SiO<sub>2</sub> and Al(OH)<sub>3</sub>.

### 2.2. Experimental Setup

Experiments were performed in laser-heated diamond anvil cells (DACs) to simulate thermodynamic parameters of the deep Earth's interior. Symmetric BX90-type DACs with culets of diameter 250 and 500  $\mu$ m were used in different experiments. A pre-indented rhenium gasket with a drilled hole was prepared as the sample chamber. The hole was filled with the powder of the Fe-bearing phase to be used in that experiment, <sup>57</sup>Fe<sub>0.94</sub>O ferropericlase or pyroxene-like glass, and small ruby chips for pressure calibration. The powder was infused with hydrocarbon liquid, which also served as a pressure medium. Pressure was measured with a Raman laser (He-Ne laser wavelength 632.8 nm, power 2 mW) from the shift of the ruby wavelength [17]. The same laser was used for Raman measurements of the sample. All sample preparation was performed at Bayerisches Geoinstitut.

A portable double-sided laser heating setup with optical fiber-based lasers (50 and 100 W) was used to produce temperatures that were measured by means of multi-wavelength spectroradiometry. The detailed setup is described in Kuppenko et al. [18]. The laser was unfocused to a spot size of  $\sim$ 20  $\mu$ m

in diameter to ensure homogeneous heating of the samples. Each heating was performed for several minutes over the entire sample in the gasket hole.

### 2.3. Analytical Techniques

Conventional Mössbauer spectroscopy with a  $^{57}\text{Co}$  point source at the Bayerisches Geoinstitut, University of Bayreuth (BGI) and the synchrotron Mössbauer source (SMS) at beamline ID18 at the European Synchrotron Radiation Facility (ESRF), Grenoble, France, were employed to monitor the electronic properties of the iron atoms as well as their local environment in the investigated systems.  $\text{K}_2\text{Mg}^{57}\text{Fe}(\text{CN})_6$  was used as a single line reference for SMS measurements and the velocity scales and isomer shifts for all Mössbauer methods were calibrated relative to  $\alpha\text{-Fe}$ . Details of the experimental procedures for high-pressure Mössbauer spectroscopic measurements are described in Kantor et al. [19], Potapkin et al. [20]. Transmission Mössbauer spectra were fitted using MossA, a program for analyzing energy-domain Mössbauer spectra from conventional and synchrotron sources that is described in Prescher et al. [21]. Spectra fitting strived to achieve good statistical fits using a minimum number of components.

High-pressure in situ powder X-ray diffraction (Figure S2) was performed on the ID09A beamline at the ESRF (MAR555 detector,  $\lambda = 0.4126\text{--}0.4130 \text{ \AA}$ ) with a beam size of dimensions  $15 \times 15 \mu\text{m}^2$  on several different spots of the sample in the gasket hole.

## 3. Results

### 3.1. Graphite And Hydrocarbons In Reaction Products

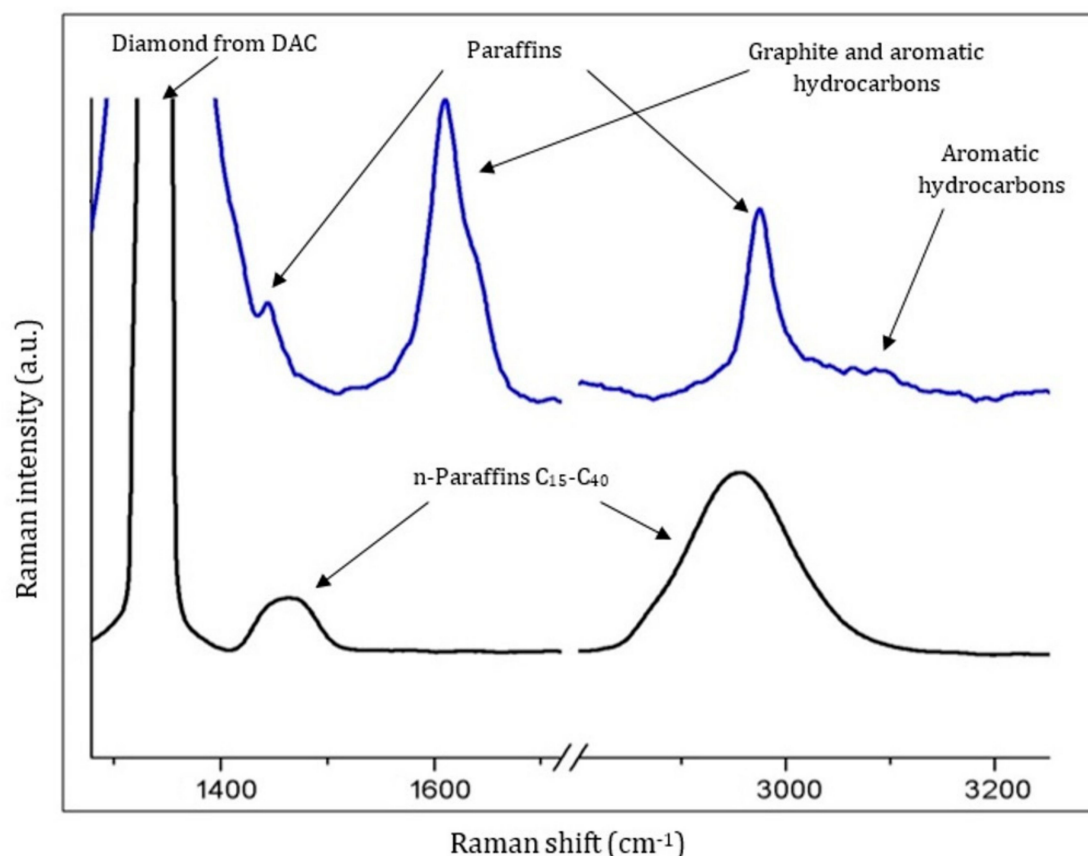
Analysis of Raman spectra of the samples of pure synthetic paraffin oil after heating to about  $1200(\pm 100) \text{ K}$  at pressures up to  $7.4(\pm 0.2) \text{ GPa}$  showed the appearance of new bands (Table 1 experiments 11–13, Figure 1). Some of the new Raman peaks can be interpreted as due to graphite. However, characteristic modes of n-alkanes (may be different from the starting material) are still present, and there are indications that new, probably aromatic, hydrocarbons are formed (Figure 1). Mössbauer spectra show that there were no chemical reactions between paraffin oil and  $\text{Fe}^{2+}$ -bearing materials (ferropericlase, for example) at conditions corresponding to slabs subducting to depths of  $\sim 200 \text{ km}$  (Table 1).

Table 1. Experimental details.

| Exp # | System   | Final P,<br>(±0.2) GPa | T,<br>(±100) K | Mössbauer Spectroscopy Results      |  | Raman Results                            | X-ray Diffraction Results  |
|-------|--|------------------------|----------------|-------------------------------------|--|--|--|
|       |  |                        |                | Rel. Area %                         | Assignment   |  |  |
| 1     | Paraffin oil + pyroxene-like glass<br>(Mg <sub>0.91</sub> Fe <sub>0.09</sub> )(Si <sub>0.91</sub> Al <sub>0.09</sub> )O <sub>3</sub> | 2.6                    | 1500           | 81.7<br>18.3                        | <i>pyroxene glass</i><br><i>FeH</i>  | Graphite                                 |  |
| 2     | Paraffin oil + pyroxene-like glass<br>(Mg <sub>0.91</sub> Fe <sub>0.09</sub> )(Si <sub>0.91</sub> Al <sub>0.09</sub> )O <sub>3</sub> | 4.5                    | 1500           | 100.0                               | <i>pyroxene glass</i>  | -  | -  |
| 3     |  |                        | 1800           | 66.4<br>33.6                        | <i>pyroxene glass</i><br><i>FeH</i>  | Graphite +<br>hydrocarbons               | orthorhombic Fe <sub>7</sub> C <sub>3</sub> + fcc FeH +<br>dhcp-FeH + graphite + clinopyroxene |
| 4     | Crude oil + ferropericlase<br>(Mg <sub>0.8</sub> Fe <sub>0.2</sub> )O  | 6.9                    | 1300           | 100.0                               | <i>ferropericlase</i>  | Fluorescence<br>typical for crude<br>oil |  |
| 5     |  |                        | 1600           | 37.8<br>34.2<br>28.0                | <i>ferropericlase</i><br><i>new Fe<sup>2+</sup> component</i><br><i>FeH</i>  |  |  |
| 6     |  |                        | 1800           | 26.1<br>53.1<br>20.8                | <i>new Fe<sup>2+</sup> component</i><br><i>FeH</i><br><i>α-Fe</i>  |  |  |
| 7     | Paraffin oil + Fe <sub>0.94</sub> O  | 7.5                    | 1200           | 100.0                               | <i>Fe<sub>0.94</sub>O</i>  | Graphite +<br>hydrocarbons               |  |
| 8     |  |                        | 1400           | 15.5<br>7.9<br>34.2<br>38.0<br>4.4  | <i>Mixed phases</i><br><i>FeH</i><br><i>Fe<sub>7</sub>C<sub>3a</sub></i><br><i>Fe<sub>7</sub>C<sub>3b</sub></i><br><i>α-Fe</i> | Graphite +<br>hydrocarbons               | orthorhombic Fe <sub>7</sub> C <sub>3</sub> + <i>dhcp</i> -FeH +<br>graphite + FeO             |
| 9     |  |                        | 1600           | 15.7<br>11.7<br>19.2<br>44.6<br>8.9 | <i>Mixed phases</i><br><i>FeH</i><br><i>Fe<sub>7</sub>C<sub>3a</sub></i><br><i>Fe<sub>7</sub>C<sub>3b</sub></i><br><i>α-Fe</i> | Graphite +<br>hydrocarbons               | orthorhombic Fe <sub>7</sub> C <sub>3</sub> + <i>dhcp</i> -FeH +<br>graphite + FeO             |

Table 1. Cont.

| Exp # | System   | Final P,<br>(±0.2) GPa | T,<br>(±100) K | Mössbauer Spectroscopy Results |                                      | Raman Results              | X-ray Diffraction Results  |
|-------|--|------------------------|----------------|--------------------------------|--------------------------------------|----------------------------|--|
|       |  |                        |                | Rel. Area %                    | Assignment                           |                            |  |
| 10    |  |                        | 2300           | 9.5                            | Mixed phases                         | Graphite +<br>hydrocarbons | orthorhombic Fe <sub>7</sub> C <sub>3</sub> + <i>dhcp</i> -FeH +<br>graphite |
|       |  |                        |                | 37.9                           | FeH                                  |                            |  |
|       |  |                        |                | 23.3                           | Fe <sub>7</sub> C <sub>3a</sub>      |                            |  |
|       |  |                        |                | 19.9                           | Fe <sub>7</sub> C <sub>3b</sub>      |                            |  |
|       |  |                        |                | 9.4                            | α-Fe                                 |                            |  |
| 11    | Paraffin oil + ferropericlase<br>(Mg <sub>0.75</sub> Fe <sub>0.25</sub> )O   | 7.4                    | 1200           | 100.0                          | <i>ferropericlase</i>                | Graphite +<br>hydrocarbons |  |
| 12    |  |                        | 1600           | 100.0                          | <i>ferropericlase</i>                | Graphite +<br>hydrocarbons |  |
| 13    |  |                        | 1800           | 53.4                           | <i>ferropericlase</i>                | Graphite +<br>hydrocarbons |  |
|       |  |                        |                | 19.2                           | FeH                                  |                            |  |
|       |  |                        |                | 19.3                           | Fe <sub>7</sub> C <sub>3</sub>       |                            |  |
|       |  |                        |                | 8.1                            | α-Fe                                 |                            |  |
|       |  |                        |                |                                |                                      |                            |  |
| 14    | Paraffin oil + pyroxene-like glass<br>(Mg <sub>0.91</sub> Fe <sub>0.09</sub> )(Si <sub>0.91</sub> Al <sub>0.09</sub> )O <sub>3</sub> | 8.8                    | 1600           | 84.6                           | <i>pyroxene glass</i>                |                            |  |
|       |  |                        |                | 11.9                           | FeH                                  |                            |  |
|       |  |                        |                | 3.5                            | Fe <sub>7</sub> C <sub>3</sub>       |                            |  |
|       |  |                        |                |                                |                                      |                            |  |
| 15    |  |                        | 2000           | 24.9                           | <i>pyroxene glass</i>                |                            |  |
|       |  |                        |                | 12.9                           | <i>new Fe<sup>3+</sup> component</i> |                            |  |
|       |  |                        |                | 36.5                           | FeH                                  |                            |  |
|       |  |                        |                | 25.6                           | Fe <sub>7</sub> C <sub>3</sub>       |                            |  |
|       |  |                        |                |                                |                                      |                            |  |
| 16    | Crude oil + ferropericlase<br>(Mg <sub>0.8</sub> Fe <sub>0.2</sub> )O  | 9.5                    | 1300           | 100.0                          | <i>ferropericlase</i>                |                            |  |
| 17    |  |                        | 1700           | 39.8                           | <i>ferropericlase</i>                |                            |  |
|       |  |                        |                | 24.9                           | FeH                                  |                            |  |
|       |  |                        |                | 22.0                           | Fe <sub>7</sub> C <sub>3a</sub>      |                            |  |
|       |  |                        |                | 11.8                           | Fe <sub>7</sub> C <sub>3b</sub>      |                            |  |
|       |  |                        |                | 1.5                            | α-Fe                                 |                            |  |



**Figure 1.** Examples of Raman spectra of paraffin oil + ferropericlase compressed to 7.4(0.2) GPa at ambient temperature (**black curve**), and after laser heating at 1200(100) K (**blue curve**). Some of the new Raman peaks can be interpreted as being due to graphite [22]. However, the characteristic modes of n-alkanes (which may be different from the starting material) are still present, and there are indications that new, probably aromatic, hydrocarbons are formed [23].

### 3.2. Formation of Iron Hydride, Iron Carbide and Graphite from Hydrocarbons and Iron-Bearing Materials

Examples of Mössbauer spectra collected on temperature-quenched samples are shown in Figure 2 (corresponding hyperfine parameters are given in Table S3). The spectrum collected after reaction between pyroxene-like glass ( $\text{Mg}_{0.91}\text{Fe}_{0.09}$ )( $\text{Si}_{0.91}\text{Al}_{0.09}$ ) $\text{O}_3$  and paraffin oil at 4.5(0.2) GPa and 1800(100) K (Figure 2a) shows a doublet (brown line) due to remaining unreacted pyroxene-like glass and a sextet (blue line) due to iron hydride dhcp-FeH [24]. Reaction between ferropericlase ( $\text{Mg}_{0.8}\text{Fe}_{0.2}$ )O and crude oil at 6.9(0.2) GPa and 1800(100) K resulted in the formation of  $\alpha$ -Fe (black sextet on Figure 2b), iron hydride dhcp-FeH [24] (blue sextet, Figure 2b), and a doublet most likely due to non-stoichiometric dhcp- $\text{FeH}_x$  or fcc- $\text{FeH}_x$  (based on the centre shift which is close to that of dhcp-FeH). Notably, no remaining ferropericlase was observed after the high-pressure high-temperature treatment. The spectra on Figure 2c show run products of the reaction between  $\text{Fe}_{0.94}\text{O}$  and paraffin oil at 7.5(0.2) GPa and 1600(100) K. The spectra are quite complex and may be deconvoluted with the following components: Sextet (black) due to  $\alpha$ -Fe, sextet (blue) due to dhcp-FeH [24], two sextets (pink) due to the orthorhombic phase of iron carbide o- $\text{Fe}_7\text{C}_3$  [25], and an asymmetric doublet (orange) with centre shift close to that of dhcp-FeH (i.e., likely from iron hydride(s) with different stoichiometry). X-ray powder diffraction data (Figure S2) also confirm the formation of dhcp-FeH together with  $\text{Fe}_7\text{C}_3$  and graphite.

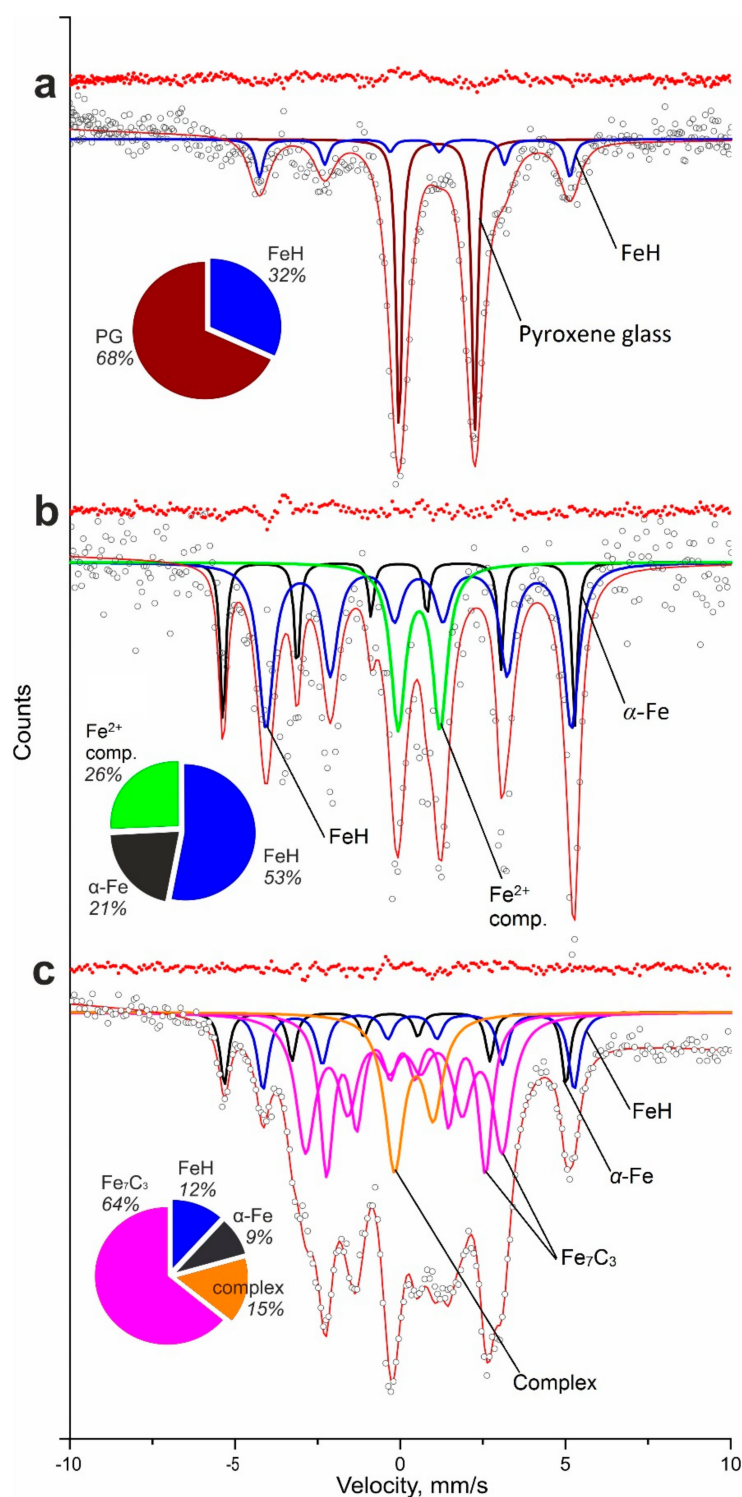


**Figure 2.** Examples of Mössbauer spectra collected at high pressure after quenching from high temperature. The following mixtures of hydrocarbons and  $\text{Fe}^{2+}$ -bearing materials were heated: (a) Pyroxene-like glass (PG) ( $\text{Mg}_{0.91}\text{Fe}_{0.09}$ )( $\text{Si}_{0.91}\text{Al}_{0.09}$ ) $\text{O}_3$  and paraffin oil heated at 4.5(0.2) GPa and 1800(100) K, (b) ferroperricite ( $\text{Mg}_{0.8}\text{Fe}_{0.2}\text{O}$ ) and crude oil at 6.9(0.2) GPa and 1800(100) K, (c) iron oxide (II)  $\text{Fe}_{0.94}\text{O}$  and paraffin oil at 7.5(0.2) GPa and 1600(100) K. Experimental points are shown by dots, fits by red lines, residuals are shown above each spectrum, and percentage sections indicate the relative amount of each component. Hyperfine parameters are given in Table S3.



Summarising the observations (Figure 3), we conclude that heating of hydrocarbons with ferrous iron oxides or silicates at temperatures above 1400 K and pressures above 2.5 GPa results in the formation of iron hydride (at pressures up to 6.9 GPa) or iron hydride and iron carbide. It is notable that the formation of iron hydride and iron carbide was observed independently of whether iron-bearing silicate or oxides were used as starting materials, although the reaction with silicate was slower, as expected. We also observed the same run products in experiments with crude oil or paraffin.

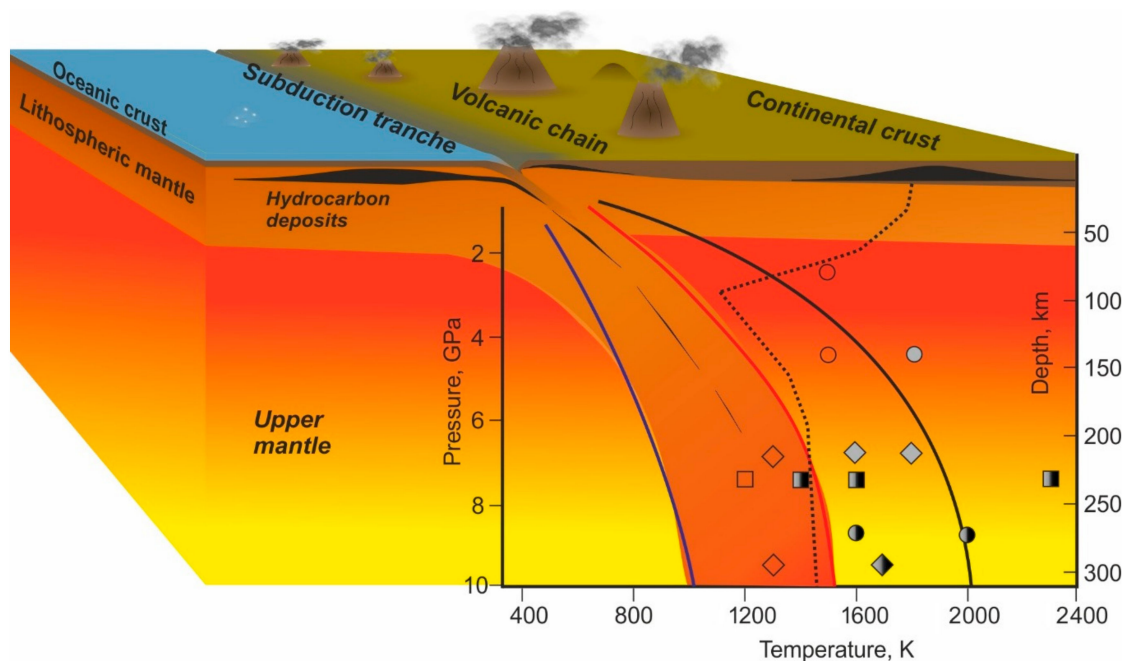


**Figure 3.** Chemical reactions between hydrocarbons and oxides and silicates. *Circles*—pyroxene-like glass ( $\text{Mg}_{0.91}\text{Fe}_{0.09})(\text{Si}_{0.91}\text{Al}_{0.09})\text{O}_3$  + paraffin oil, *diamonds*—ferropericlase ( $\text{Mg}_{0.8}\text{Fe}_{0.2})\text{O}$  + crude oil, *squares*—iron oxide (II)  $\text{Fe}_{0.94}\text{O}$  + paraffin oil, *open symbols*—no reaction, *shaded grey*—iron hydride present in the run product, *shaded black*—iron hydride and iron carbide are present in the run product. Pressure-temperatures profiles of the coldest (blue solid line) and the hottest (red solid line) subduction slabs are taken from Karato [9]. Earth's geotherm (black solid line) is modified after Pollack and Chapman [26] and the black dashed line is the melting curve of  $\gamma\text{-FeH}_x$  [27].

## 4. Discussion

### 4.1. Influence of Starting Iron-Bearing Material and Oxygen Fugacity on the Yield of Iron Hydride

Formation of iron hydrides  $\text{FeH}_x$  ( $x = 1\text{--}3$ ) as a direct reaction of iron and hydrogen has been observed at pressures up to 80 GPa and temperatures up to 1600 K [24,28–31]. Iron hydrides with different compositions have also been found to be stable at ambient temperature and pressure well above 150 GPa [24,28–30,32]. Iron hydride (fcc- $\text{FeH}_x$ ) has been synthesized by reaction of paraffin oil and pure iron over a wide range of pressures (40 to 80 GPa) upon laser heating in the DAC [30]. Our experiments demonstrate that iron hydride could be a product of chemical reactions of natural hydrocarbons and oxides and/or silicates at conditions relevant to subducting slabs (Figure 3). Moreover, we observed iron hydride even in experiments with an obvious excess of oxides or silicates, indicating that  $\text{FeH}_x$  may be stable over a large range of oxygen fugacity.

### 4.2. Depth Intervals of Iron Hydride and Iron Carbide Formation, According to Slab Geotherms

Studies on iron carbides have demonstrated their stability at pressures up to 250 GPa and temperatures up to 4100 K [33–35]. Iron carbides have already been considered to be good candidates as accessory phases in the lower mantle [4] or important components of the core [25]. According to our



observations (Table 1), iron carbides may be formed due to the interaction between hydrocarbons and different types of rock-forming materials containing ferrous iron during slab subduction. The minimum depth for iron carbide formation is found to be approximately 180–200 km. At greater depths, iron hydrides could co-exist with carbides.

Our experimental observations can be generalized as follows. As temperature increases to 1350(±100) K at pressures between 2.6(±0.2) and 6.9(±0.2) GPa (which corresponds to depths of 80–200 km), hydrocarbons react with rock-forming minerals present in the slab to form iron hydride (“FeH”, which refers to a wide range of hydrides with variable amounts of hydrogen). At higher pressures (up to 9.5(±0.2) GPa, i.e., depths down to 300 km), iron carbide(s) can additionally be formed.

#### 4.3. $\alpha$ -Fe in the Reaction Products

Pure iron found in some of our experiments is most probably an intermediate product which has not (yet) reacted with hydrogen or carbon. The amount of iron hydride increases with increasing temperature at the expense of iron carbide(s), indicating that part of the carbide(s) may react to form hydride(s) (experiments 8–10, Table 1). Notably, the amount of iron hydride in the run products could reach 50 vol. % (experiment 6, Table 1).

#### 4.4. Formation of Iron Hydride Phase in Mantle

Iron hydride that forms as a result of chemical interaction of subducted hydrocarbons and the surrounding (or reservoir) rocks has a low melting temperature (Figure 3) (even compared to slab temperatures). The density of iron hydride (~7.3–7.5 g/cm<sup>3</sup> at pressures of 4–10 GPa [28]) is significantly higher than the density of surrounding silicate-bearing rocks (3.3 g/cm<sup>3</sup> at depths of 200 km, according to PREM). Thus, iron hydride (probably together with iron carbide) may form a negatively buoyant single phase that could sink to greater depths, thus providing a source of hydrogen and reduced iron to the deep Earth’s interior. Therefore, iron hydrides probably still play a significant role in global elemental geochemical cycles on Earth.

## 5. Conclusions

Our study demonstrated the transformation of hydrocarbon systems during subduction and their chemical interaction with the iron-bearing surrounding. It was shown that iron carbide (Fe<sub>7</sub>C<sub>3</sub>) and iron hydride (FeH) may be formed from this interaction at the mantle thermobaric conditions at the depth of 200–290 km and in a wide range of oxygen fugacity. These substances may be present in the mantle and take part in other abyssal processes, such as global elemental cycles and deep hydrocarbons formation.

**Supplementary Materials:** The following are available online at <http://www.mdpi.com/2075-163X/9/11/651/s1>, Figure S1: Raman spectra of the complex hydrocarbons system at 1.4(0.2) GPa and ambient temperature (red curve) and after heating for 12 h at 723(10) K (black curve), Figure S2: Examples of X-ray diffraction patterns collected on temperature-quenched samples in DACs at different pressures that have been processed by Rietveld refinements using full-profile GSAS software. (a) Glass of pyroxene composition + paraffin after heating at 4.5(1) GPa and 1800(100) K, (b) wüstite (FeO) + paraffin after heating at 7.5(2) GPa and 1400(100) K. While interpretation of the complex diffraction patterns on their own are ambiguous, phase assignments are more robust in combination with results of Mössbauer and Raman spectroscopies, Table S1: Characteristics of paraffin oil (from Merck KGaA, EMD Millipore Chemical 1.07160.1000), Table S2: Characteristics of crude oil from the Korchaginское deposit (Astrakhan region). Table S3: Hyperfine parameters of Mossbauer spectra (for Figure 2).

**Author Contributions:** V.K. and L.D. designed the study. L.D. designed the experiments. A.S., E.M., D.K., G.A. and L.D. carried out the experiments and analysed the data. I.K., A.C. (Aleksandr Chumakov) and M.H. helped with synchrotron experiments. A.S., E.M., V.K., and A.C. (Aleksey Chernoutsan) wrote the manuscript with substantial contributions made by the L.D. and C.M. All authors discussed the results and implications and commented on the manuscript.

**Funding:** This research received no external funding.

**Acknowledgments:** We thank A. Kurnosov for valuable information and comments during experiments. We thank D. Vasyukov, R. Rüffer and V. Cerantola for their help during Mössbauer experiments. We thank E. Bykova, M. Bykov and L. Ismailova for providing their help during X-ray measurements. We acknowledge the European Synchrotron Radiation Facility for provision of synchrotron radiation facilities at the beamline ID18.

**Conflicts of Interest:** The authors declare no conflict of interest.

## References

1. Sverjensky, D.A.; Stagno, V.; Huang, F. Important role for organic carbon in subduction-zone fluids in the deep carbon cycle. *Nat. Geosci.* **2014**, *7*, 909–913. [[CrossRef](#)]
2. Facq, S.; Daniel, I.; Montagnac, G.; Cardon, H.; Sverjensky, D.A. In situ Raman study and thermodynamic model of aqueous carbonate speciation in equilibrium with aragonite under subduction zone conditions. *Geochim. Cosmochim. Acta* **2014**, *132*, 375–390. [[CrossRef](#)]
3. Galvez, M.E.; Beyssac, O.; Martinez, I.; Benzerara, K.; Chaduteau, C.; Malvoisin, B.; Malavieille, J. Graphite formation by carbonate reduction during subduction. *Nat. Geosci.* **2013**, *6*, 473–477. [[CrossRef](#)]
4. Dasgupta, R.; Mallik, A.; Tsuno, K.; Withers, A.C.; Hirth, G.; Hirschmann, M.M. Carbon-dioxide-rich silicate melt in the Earth's upper mantle. *Nature* **2013**, *493*, 211–222. [[CrossRef](#)] [[PubMed](#)]
5. Kopf, A.J. Significance of mud volcanism. *Rev. Geophys.* **2002**, *40*, 2-1–2-52. [[CrossRef](#)]
6. Evans, K.A. The redox budget of subduction zones. *Earth Sci. Rev.* **2012**, *113*, 11–32. [[CrossRef](#)]
7. Bataleva, Y.V.; Palyanov, Y.N.; Borzdov, Y.M.; Bayukov, O.A.; Zdrokov, E.V. Iron carbide as a source of carbon for graphite and diamond formation under lithospheric mantle P-T parameters. *Lithos* **2017**, *286–287*, 151–161. [[CrossRef](#)]
8. Mann, P.; Gahagan, L.; Gordon, M.B. Tectonic Setting of the World's Giant Oil and Gas Fields. In *Giant Oil and Gas Fields of the Decade 1990-1999*; AAPG Datapage: Tulsa, OK, USA, 2003; pp. 15–105.
9. Karato, S.-I. *Physics and Chemistry of the Deep Earth*; Karato, S.-I., Ed.; John Wiley & Sons: Hoboken, NJ, USA, 2013; p. 416.
10. Langdon, S.P.; Connor, J.K.; Chandler, R.B.; Jellison, M.J. Deepwater Drilling Challenges Demonstrate Learning Curve with New Connection Technology. In Proceedings of the 2010 IADC/SPE Drilling Conference and Exhibition, New Orleans, LO, USA, 2–4 February 2010. [[CrossRef](#)]
11. Serovaiskii, A.Y. Investigation of stability of the model hydrocarbon system at thermobaric conditions, corresponding to depth down to 50 km. In Proceedings of the “Bakirovskie chteniya” conference, Moscow, Russia, 1 March 2018.
12. Kolesnikov, A.; Kutcherov, V.G.; Goncharov, A.F. Methane-derived hydrocarbons produced under upper-mantle conditions. *Nat. Geosci.* **2009**, *2*, 566–570. [[CrossRef](#)]
13. Kenney, J.F.; Kutcherov, V.A.; Bendeliani, N.A.; Alekseev, V.A. The evolution of multicomponent systems at high pressures: VI. The thermodynamic stability of the hydrogen-carbon system: The genesis of hydrocarbons and the origin of petroleum. *Proc. Nalt. Acad. Sci. USA* **2002**, *99*, 10976–10981. [[CrossRef](#)]
14. Kutcherov, V.G.; Kolesnikov, A.; Dyugheva, T.I.; Kulikova, L.F.; Nikolaev, N.N.; Sazanova, O.A.; Braghkin, V.V. Synthesis of complex hydrocarbon systems at temperatures and pressures corresponding to the Earth's upper mantle conditions. *Dokl. Phys. Chem.* **2010**, *433*, 132–135. [[CrossRef](#)]
15. Frost, D.J.; McCammon, C.A. The redox state of Earth's mantle. *Annu. Rev. Earth Planet. Sci.* **2008**, *36*, 389–420. [[CrossRef](#)]
16. Sinmyo, R.; Glazyrin, K.; McCammon, C.; Kuppenko, I.; Kantor, A.; Potapkin, V.; Chumakov, A.I.; Rüffer, R.; Dubrovinsky, L. The influence of solid solution on elastic wave velocity determination in (Mg,Fe)O using nuclear inelastic scattering. *Phys. Earth Planet. Inter.* **2014**, *229*, 16–23. [[CrossRef](#)]
17. Dewaele, A.; Datchi, F.; Loubeyre, P.; Mezouar, M. High pressure-high temperature equations of state of neon and diamond. *Phys. Rev. B* **2008**, *77*, 094106. [[CrossRef](#)]
18. Kuppenko, I.; Dubrovinsky, L.; Dubrovinskaya, N.; McCammon, C.; Glazyrin, K.; Bykova, E.; Ballaran, T.B.; Sinmyo, R.; Chumakov, A.I.; Potapkin, V.; et al. Portable double-sided laser-heating system for Mossbauer spectroscopy and X-ray diffraction experiments at synchrotron facilities with diamond anvil cells. *Rev. Sci. Instrum.* **2012**, *83*, 124501. [[CrossRef](#)]

19. Kantor, I.; Prakapenka, V.; Kantor, A.; Dera, P.; Kurnosov, A.; Sinogeikin, S.; Dubrovinskaia, N.; Dubrovinsky, L. BX90: A new diamond anvil cell design for X-ray diffraction and optical measurements. *Rev. Sci. Instrum.* **2012**, *83*, 125102. [[CrossRef](#)]
20. Potapkin, V.; Chumakov, A.I.; Smirnov, G.V.; Ruffer, R.; McCammon, C.; Dubrovinsky, L. Angular, spectral, and temporal properties of nuclear radiation from a Fe-57 synchrotron Mossbauer source. *Phys. Rev. A* **2012**, *86*, 053808. [[CrossRef](#)]
21. Prescher, C.; McCammon, C.; Dubrovinsky, L. MossA: A program for analyzing energy-domain Mossbauer spectra from conventional and synchrotron sources. *J. Appl. Crystallogr.* **2012**, *45*, 329–331. [[CrossRef](#)]
22. Hanfland, M.; Beister, H.; Syassen, K. Graphite under pressure: Equation of state and first-order Raman modes. *Phys. Rev. B* **1989**, *39*, 12598. [[CrossRef](#)]
23. Sterin, K.E.; Aleksanyan, V.; Zhizhin, G.N. *Raman Spectra of Hydrocarbons*; Elsevier: Amsterdam, The Netherlands, 2013.
24. Narygina, O.; Dubrovinsky, L.S.; McCammon, C.A.; Kurnosov, A.; Kantor, I.Y.; Prakapenka, V.B.; Dubrovinskaia, N.A. X-ray diffraction and Mössbauer spectroscopy study of fcc iron hydride FeH at high pressures and implications for the composition of the Earth's core. *Earth Planet. Sci. Lett.* **2011**, *307*, 409–414. [[CrossRef](#)]
25. Prescher, C.; Dubrovinsky, L.; Bykova, E.; Kuppenko, I.; Glazyrin, K.; Kantor, A.; McCammon, C.; Mookherjee, M.; Nakajima, Y.; Miyajima, N.; et al. High Poisson's ratio of Earth's inner core explained by carbon alloying. *Nat. Geosci.* **2015**, *8*, 220–223. [[CrossRef](#)]
26. Pollack, H.N.; Chapman, D.S. On the regional variation of heat flow, geotherms, and lithospheric thickness. *Tectonophysics* **1977**, *38*, 279–296. [[CrossRef](#)]
27. Sakamaki, K.; Takahashi, E.; Nakajima, Y.; Nishihara, Y.; Funakoshi, K.; Suzuki, T.; Fukai, Y. Melting phase relation of FeH<sub>x</sub> up to 20 GPa: Implication for the temperature of the Earth's core. *Phys. Earth Planet. Inter.* **2009**, *174*, 192–201. [[CrossRef](#)]
28. Badding, J.V.; Hemley, R.J.; Mao, H.K. High-pressure chemistry of hydrogen in metals—In situ study of iron hydride. *Science* **1991**, *253*, 421–424. [[CrossRef](#)] [[PubMed](#)]
29. Fukai, Y.; Yamakata, M.; Yagi, T. Some High-Pressure Experiments on the Fe-H System. *Z. Phys. Chem.* **1993**, *179*, 119–123. [[CrossRef](#)]
30. Yamakata, M.; Yagi, T.; Utsumi, W.; Fukai, Y. In situ X-ray Observation of Iron Hydride under High Pressure and High Temperature. *Proc. Jpn. Acad. Ser. B* **1992**, *68*, 172–176. [[CrossRef](#)]
31. Pépin, C.M.; Dewaele, A.; Geneste, G.; Loubeyre, P.; Mezouar, M. New Iron Hydrides under High Pressure. *Phys. Rev. Lett.* **2014**, *113*, 265504. [[CrossRef](#)]
32. Shibazaki, Y.; Terasaki, H.; Ohtani, E.; Tateyama, R.; Nishida, K.; Funakoshi, K.-i.; Higo, Y. High-pressure and high-temperature phase diagram for Fe<sub>0.9</sub>Ni<sub>0.1</sub>-H alloy. *Phys. Earth Planet. Inter.* **2014**, *228*, 192–201. [[CrossRef](#)]
33. Lord, O.T.; Walter, M.J.; Dasgupta, R.; Walker, D.; Clark, S.M. Melting in the Fe-C system to 70 GPa. *Earth Planet. Sci. Lett.* **2009**, *284*, 157–167. [[CrossRef](#)]
34. Nakajima, Y.; Takahashi, E.; Suzuki, T.; Funakoshi, K. "Carbon in the core" revisited. *Phys. Earth Planet. Inter.* **2009**, *174*, 202–211. [[CrossRef](#)]
35. Takahashi, S.; Ohtani, E.; Sakai, T.; Mashino, I.; Kamasda, S.; Miyahara, M.; Sakamaki, T.; Hirao, N.; Ohishi, Y. Stability and melting relations of Fe<sub>3</sub>C up to 3 Mbar: Implication for the carbon in the Earth's inner core. In Proceedings of the American Geophysical Union, San Francisco, CA, USA, 9–13 December 2013.

